PAPER
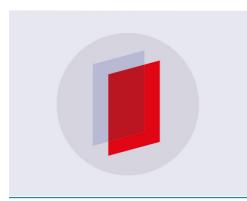
Comparison of thermal conductance of graphene/SiO_2 and graphene/Au interfaces based on Raman optothermal method

View the article online for updates and enhancements.

IOP ebooks™

Bringing you innovative digital publishing with leading voices to create your essential collection of books in STEM research.

Start exploring the collection - download the first chapter of every title for free.

Materials Research Express

Comparison of thermal conductance of graphene/SiO$_2$ and graphene/Au interfaces based on Raman optothermal method

Yanru Xu[1], Jin Jiang[1,6], Bo Yang[2], Maodong Li[2], Shen Xu[3,6] and Yanan Yue[1,4,5,6]

[1] Key Laboratory of Hydraulic Machinery Transients (MOE), School of Power and Mechanical Engineering, Wuhan University, Wuhan, Hubei 430072, People's Republic of China
[2] National Graphene Center (Guangdong), Guangzhou Special Pressure Equipment Inspection and Research Institute, Guangzhou 510663, People's Republic of China
[3] School of Mechanical and Automotive Engineering, Shanghai University of Engineering Science, Shanghai 201620, People's Republic of China
[4] Department of Mechanical Engineering, Boston University, Boston, Massachusetts 02215, United States of America
[5] Department of Mechanical and Manufacturing Engineering, Miami University, Oxford, Ohio 45056, United States of America
[6] Authors to whom any correspondence should be addressed.

E-mail: jiangjing423@163.com, shxu16@sues.edu.cn and yyue@whu.edu.cn

Keywords: graphene/silicon oxide, graphene/gold, Raman optothermal method, interfacial thermal conductance

Abstract

Due to the atom-scale thickness and the large surface area to volume ratio, the interfacial thermal conductance between graphene (Gr) and substrates is a critical property for thermal management application of graphene into micro/nano scale electronic devices. It has been widely proved to be dependent on the interfacial phonons transport, material morphology, and interfacial force. The material category of the substrate is related to the interfacial thermal conductance, but, the experimental studies of which are lacking. In this work, the thermal conductance (G) of Gr on SiO$_2$ and Au substrates is measured using Raman optothermal approach combined with finite element simulations. $G_{\mathrm{Gr/SiO2}}$ is determined to be $7.7^{+0.7}_{-0.6} \times 10^3$ W $\cdot$ m^{-2} $\cdot$ K^{-1}, while $G_{\mathrm{Gr/Au}}$ is $(1.7 \pm 0.2) \times 10^4$ W $\cdot$ m^{-2} $\cdot$ K^{-1}. They are in the same order of magnitude, but $G_{\mathrm{Gr/Au}}$ is a little larger than twice of $G_{\mathrm{Gr/SiO2}}$. Compared with the elastic-phonon-scattering-dominated heat transfer across the Gr/SiO$_2$ interface, the interfacial thermal conductance of Gr/Au is enhanced by the increased probability of multi-phonons inelastic scatterings due to the lower Debye temperature of Au than the ambient temperature and the additional contribution from electron scatterings. Besides, the interfacial adhesion energy of Gr/Au is higher than that of Gr/SiO$_2$ which contributes to $G_{\mathrm{Gr/Au}}$ larger than $G_{\mathrm{Gr/SiO2}}$. The metallic substrate like Au will benefit the heat transfer across graphene interfaces, with respect to the nonmetallic substrate like SiO$_2$. Our results offer new insights into the interfacial heat transfer mechanisms between graphene and nonmetallic (or metallic) substrates. They also provide guidance for tuning the interfacial heat transfer in applications of 2D materials in thermal management of compact devices by switching the material category of substrates.

1. Introduction

As the first discovered two-dimensional atomic crystal material, graphene has drawn enormous research and application interests. It is a single layer of carbon atoms arranged in a honeycomb lattice and exhibits a high intrinsic in-plane thermal conductivity (exceeding 3000 W $\cdot$ m^{-1} $\cdot$ K^{-1} [1]). With the significant miniaturization and high-power densification, the high efficiency of heat removal has become an emerging demand for micro/nano electronic devices [2]. Graphene shows a great potential in thermal management due to its high thermal conductivity and good mechanical properties and flatness. Due to the atom-thick structure and the large surface area to volume ratio, the thermal transport of graphene is strongly affected by supporting substrates. Similar as the electron mobility (2.5×10^5 cm^2 $\cdot$ V^{-1} $\cdot$ s^{-1} [3]) of graphene, which could be limited to 4×10^4 cm^2 $\cdot$ V^{-1} $\cdot$ s^{-1} by the extrinsic scattering of surface phonons of SiO$_2$ [4] when graphene is placed on

SiO$_2$ substrate, the in-plane thermal conductivity of graphene could also be reduced by an order of magnitude due to the contacts with SiO$_2$ substrate [5]. The increase in phonon scatterings at the interface will reduce the relaxation time of heat-conducting phonons and result in the reduction of heat transport in plane [6]. Phonons carrying thermal energy across the interface [7] lead to heat dissipation. Therefore, the interfacial heat transfer of graphene is a significant issue for its application into micro/nano scale electronic devices [8]. Thermal conductance of the interface between graphene and substrates becomes a critical property deciding its thermal performance [2].

Heat transfer across graphene interface has been found to be related to the interactions, the crystallinity of substrate, and chemical functionalization. Compared with the van der Waals interface, the graphene interface via covalent bonds has larger thermal conductance. It has been proved by empirical molecular dynamic simulations on the thermal transport across graphene/4H-SiC interface [9]. The crystallinity of substrate is another factor affecting the thermal conductance of graphene interface [9]. The graphene/a-SiC interface has a higher thermal conductance than the graphene/c-SiC interface. The studies on the thermal properties of hydrogenated graphene and oxidized graphene [10, 11] demonstrated that the interfacial thermal conductance could be tailored by adjusting the hydrogen or oxygen coverage on graphene. Till now, to our best knowledge, there is no experimental study on the interfacial thermal conductance between the same graphene and metallic substrate or nonmetallic substrate. The effect of material category of substrates on the interfacial thermal conductance is still unknown. It is necessary to conduct comparative thermal characterization of graphene supported on different substrates. The thermoreflectance method, a commonly measure applied to sandwiched interfaces measurement, inevitably includes metallic heaters [10, 12], and the heater-induced effect could be hardly excluded. In order to compare the interfacial thermal conductance between the same graphene on different substrates, Raman optothermal method could be competent.
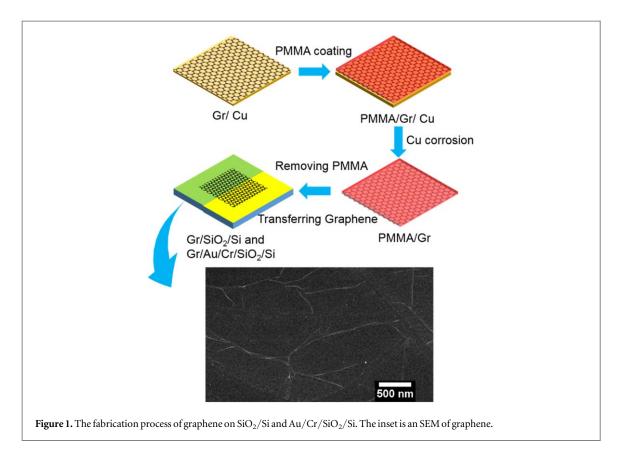
Raman signal of graphene has a significant feature of temperature-dependence. Balandin *et al* [13] firstly experimentally measured super-high thermal conductivity in graphene by using Raman method. For its in-situ and contact-free advantages, Raman thermometry has been widely used to investigate the thermal properties of graphene [14, 15], carbon nanotubes [16–18], MoS$_2$ [19], WS$_2$ [20] and other low dimensional materials [21–24]. Our group has also successfully applied this technique to thermally characterize the graphene/SiC interface [25] and carbon nanotube fibers [26]. In this work, Raman optothermal method is employed to probe the temperature of graphene on SiO$_2$ and Au, and then to derive the thermal conductance of the two types of graphene interfaces combined with finite element (FE) simulations. The peak shift of the G band is used as the temperature probe. The reliability of the temperature measurement is ensured by using a large laser spot size and a low laser intensity. The used spot size of 50 μm in diameter is much larger than the thermalization length of ZA and other acoustic and optical phonon polarizations [27], and can significantly reduce the degree of nonequilibrium [28, 29]. The laser intensity is 0.015 mW $\cdot$ μm^{-2}, three orders of magnitude lower than the threshold value (19.66 mW $\cdot$ μm^{-2}) of observing the nonequilibrium by Raman measurements [27], so the degree of phonons nonequilibrium could be neglected.
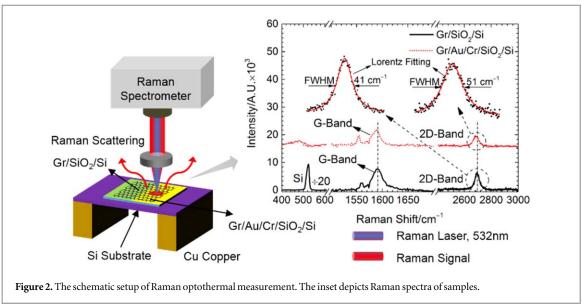
2. Sample preparation and Raman optothermal characterization details

2.1. Sample preparation and characterization

A 200-nm-thick gold film (99.99%) is partially deposited on a 2 cm $\times$ 2 cm SiO$_2$/Si substrate by sputtering coating method in a vacuum chamber. The adhesion layer is a 20-nm-thick Cr film. The used coating rate is 0.02 $\sim$ 0.06 nm s^{-1} and vacuum pressure 2.7 $\sim$ 2.8 $\times$ 10^{-4} Pa. The obtained substrate is denoted as Au/Cr/SiO$_2$/Si. The single layer graphene (denoted as Gr) is grown on a Cu foil by chemical vapor deposition method (CVD) in a tube furnace [30] (denoted as Gr/Cu). Gr/Cu is wetly transferred onto the surface of SiO$_2$ and Au, as shown in figure 1. A layer of polymethylmethacrylate (PMMA) is coated onto the surface of Gr/Cu as a supporting layer (denoted as PMMA/Gr/Cu). PMMA/Gr/Cu is then immersed in a CuSO$_4$/FeCl$_3$ solution to etch Cu. The remaining PMMA/Gr is carefully transferred in a deionized water bath to remove the residual etchant. The target substrate is used to lift the PMMA-supported graphene from the water bath. After the sample is dried, the PMMA layer is removed by rinsing the sample with acetone solution and alcohol solution accordingly. Finally, the target regions of Gr/SiO$_2$ and Gr/Au on silicon substrate are obtained.

Graphene is characterized using Zeiss SIGMA scanning electron microscopy. The SEM image of graphene is shown in figure 1. Corrugations and ripples in graphene are inevitably induced in CVD prepared and wetly transferred graphene [31]. The Raman spectrum of graphene is characterized by a B&W Tek Raman spectroscopy with an excitation laser of 532 nm. The applied integration time is 160 s and the laser power is 30 mW. Raman spectra of graphene on SiO$_2$ and Au are both shown in figure 2, showing G band ($\sim$1591 cm^{-1}, in-plane vibrational mode of sp^2 carbon atoms similar as graphite) and 2D band ($\sim$2700 cm^{-1}, double resonance mode of phonons) [32]. No D band appearing in the spectra indicates the absence of structural disorders and

Figure 1. The fabrication process of graphene on SiO$_2$/Si and Au/Cr/SiO$_2$/Si. The inset is an SEM of graphene.

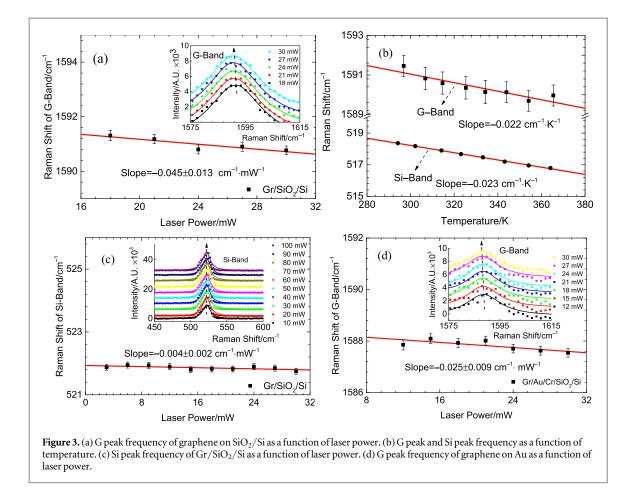**Figure 2.** The schematic setup of Raman optothermal measurement. The inset depicts Raman spectra of samples.

defects in graphene. A weak band at 1554 $\sim$ 1560 cm^{-1} may be attributed to the hybridization of carbon bonds [33]. The Raman spectrum of Gr/SiO$_2$/Si exhibits the first-order band of silicon at 521 cm^{-1}. The full width at half-maximum (FWHM) of 2D band fitted by the Lorentzian function is 41 cm^{-1}, 51 cm^{-1} for graphene on SiO$_2$ and Au, respectively. They are both between that of single layer graphene ($\sim$30 cm^{-1}) and double-layer graphene ($\sim$60 cm^{-1}) [34], indicating the prepared graphene monolayer. The intensity ratio of 2D band to G band is 0.79 and 0.74 for graphene on SiO$_2$ and Au, respectively. Both of them are lower than 1, which may be attributed to that the focal spot size is large enough that the sample region with corrugations and ripples could be covered.

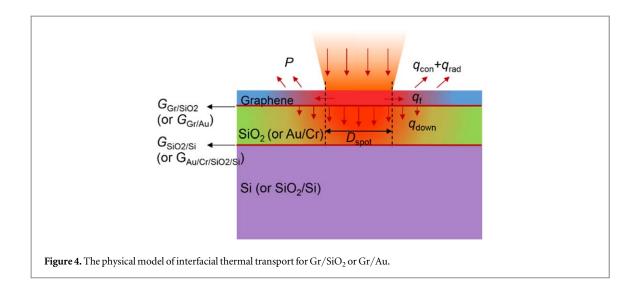## 2.2. Raman optothermal characterization details

The measurement scheme of Raman optothermal method is shown in figure 2. The same Raman spectrometer mentioned above is used. The diameter of laser focal spot is approximately 50 μm. The Raman spectrometer's spectral range is from 15 to 3000 cm^{-1} in Raman frequency. The same focal level is used to heat graphene on

Figure 3. (a) G peak frequency of graphene on SiO_2/Si as a function of laser power. (b) G peak and Si peak frequency as a function of temperature. (c) Si peak frequency of $Gr/SiO_2/Si$ as a function of laser power. (d) G peak frequency of graphene on Au as a function of laser power.
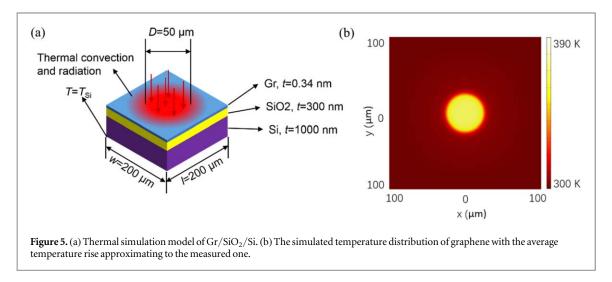
SiO_2 and Au. The laser power is adjusted from 18 to 30 mW. In order to collect sound spectra, the corresponding integration time is set as 10 s to 160 s. Under each power, three groups of spectra are collected and all the experiments are repeated to reduce the temperature measurement uncertainty. The specific peak position of G band is fitted by the Lorentzian function, and further used to determine the temperature of graphene. Since the temperature coefficient of Raman peak is related to the sample quality and laser wavelength, it is determined by a calibration over the temperature range from 294 to 365 K. At each steady temperature, three groups of signals are collected and all the experiments are repeated once for averaging.

For the graphene on SiO_2, as shown in the inset of figure 3(a), the fitted line of G band shifts to a lower wavenumber as the laser power increases. G peak frequency (Raman shift) decreases linearly against the laser power, with a slope of $-0.045 \pm 0.013 \ cm^{-1} \cdot mW^{-1}$ as shown in figure 3(a). The calibration result is shown in figure 3(b). The temperature coefficient of G band is fitted as $-0.022 \ cm^{-1} \cdot K^{-1}$, approximating to the reported value of $-0.024 \ cm^{-1} \cdot K^{-1}$ [35]. Based on this, the temperate rise of graphene within the focal region is $\Delta T_{Gr} = 61.4 \pm 3.2 \ K$ at the laser power of 30 mW. The variation of Si band against the laser power is shown in figure 3(c). The fitted Si peak frequency of silicon covered by graphene shows a blueshift of $3 \ cm^{-1}$ with respect to the bare silicon in figure 3(b) at ambient temperature, which could be attributed to the phonon confinement effect and residue surface strain [36]. As laser power increases, Si peak frequency shows a redshift from $521.93 \ cm^{-1}$ to $521.81 \ cm^{-1}$, with a fitted slope of $-0.004 \pm 0.002 \ cm^{-1} \cdot mW^{-1}$. The temperature coefficient of Si band is shown in figure3(b), fitted as $-0.023 \ cm^{-1} \cdot K^{-1}$, similar as the reported value of $-0.022 \ cm^{-1} \cdot K^{-1}$ [37]. With this slope, the temperature rise of the silicon top surface is $\Delta T_{Si} = 5.2 \pm 1.1 \ K$ at laser power of 30 mW.

Figure 3(d) shows the shifting of G peak frequency of graphene on Au at different laser powers. The fitted slope between G peak frequency and the laser power is $-0.025 \pm 0.009 \ cm^{-1} \cdot mW^{-1}$. Based on the temperature coefficient of G band ($-0.022 \ cm^{-1} \cdot K^{-1}$), the temperate rise of graphene within the focal region is $\Delta T_{Gr} = 34.1 \pm 3.6 \ K$ at laser power of 30 mW. Since Au is not Raman-active, the temperature of Au could not be directly measured using Raman thermometry. The surface temperature of the silicon substrate cannot be probed neither due to the fact that Au layer is thicker than the optical penetration depth ($\sim 104 \ nm$) of Au at 532 nm. No beam of the incident laser would reach the bottom surface of silicon, and its temperature is around room temperature.

Figure 4. The physical model of interfacial thermal transport for Gr/SiO$_2$ or Gr/Au.

Figure 5. (a) Thermal simulation model of Gr/SiO$_2$/Si. (b) The simulated temperature distribution of graphene with the average temperature rise approximating to the measured one.

3. Thermal transport simulation and interface conductance determination
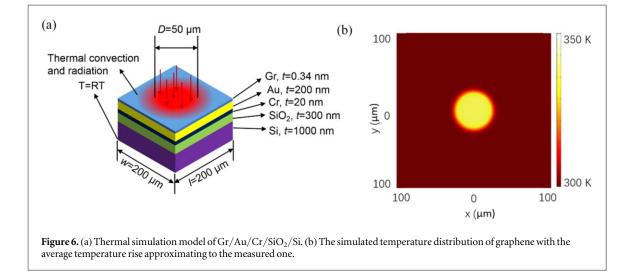
3.1. Physical model development

The physical model of the interfacial thermal transport is shown in figure 4. A simulated heating source in graphene imitates the photon energy absorption from the irradiation of the incident laser beam. Heat transfers both in plane and across the Gr/SiO$_2$ or Gr/Au interface into the substrate. The boundary conditions of heat convection and heat radiation are applied to the upper surface of graphene, as part of thermal energy dissipating to surroundings on the surface. The temperature of the graphene and substrate measured by Raman optothermal method are used as a criteria to evaluate the simulation result. Then, the thermal conductance of graphene interface G can be extracted when the simulated average temperature of graphene within the heated region approximates to the measured value.

A steady-state thermal FE model is built. The governing equation for steady-state heat transfer of graphene in the cylindrical coordinates [38] is

$$\frac{1}{r}\frac{\mathrm{d}}{\mathrm{d}r}\left(r\frac{\mathrm{d}T}{\mathrm{d}r}\right) - \frac{G_{\mathrm{Gr}}}{k_{\mathrm{Gr}}t_{\mathrm{Gr}}}(T - T_a) + \frac{\dot{q}_{\mathrm{Gr}}}{k_{\mathrm{Gr}}} = 0 \tag{1}$$

Where r is the radius with respect to the center of the laser beam, G_{Gr} is the thermal conductance of graphene/ substrate, k_{Gr} is the thermal conductivity of graphene, t_{Gr} is the thickness of monolayer graphene (0.34 nm) [39], T_a is the ambient temperature of 300 K, and $\dot{q}_{\mathrm{Gr}}$ is the volumetric optical heat source in graphene.

The geometry of the simulation model is shown in figures 5(a) and 6(a), respectively. The simulation results show that graphene temperatures converge with the width and length of graphene and substrate varying from 200 μm to 1000 μm. Thus, the width and length of graphene and substrate are all set to be 200 μm. The depth of silicon is set to be 1000 nm, which is also proved to meet the convergence requirement. In order to ensure the convergence of solution with reasonable computational time, the mesh size ranges from 0.17 nm to 30 μm. The

Figure 6. (a) Thermal simulation model of Gr/Au/Cr/SiO$_2$/Si. (b) The simulated temperature distribution of graphene with the average temperature rise approximating to the measured one.

Table 1. Properties of materials used in the simulation.

	Density (kg · m^{-3})	Thermal conductivity (W · m^{-1} · K^{-1})	Constant pressure heat capacity (J · (kg · K)$^{-1}$)
Gr	2200 [40]	179 [41]	750 [40]
SiO$_2$	2200	1.4 [42]	730
Si	2329	130	700
Au	19300	317	129
Cr	7150	93.7	448

denser mesh is used in the thin graphene and the coarser mesh is used in the thick substrate. The convective heat transfer coefficient is set to be 10 W · m^{-2} · K^{-1}. The emissivity of graphene is set as 0.023. Table 1 lists the material properties used in the simulation.

3.2. Thermal conductance of Gr/SiO$_2$ interface

The FE simulation model of Gr/SiO$_2$/Si is shown in figure 5(a). A uniform heat source $\dot{q}_{\mathrm{Gr/SiO2}}$ is applied to the heated region in graphene expressed as $\dot{q}_{\mathrm{Gr/SiO2}} = \alpha_{\mathrm{Gr/SiO2}} I / t_{\mathrm{Gr}}$, where $\alpha_{\mathrm{Gr/SiO2}}$ is the absorptance of graphene on SiO$_2$. The intrinsic optical absorptance of monolayer graphene is 2.3% in the visible range of wavelength [43]. Considering the reflectance of SiO$_2$ is 40% [41], $\alpha_{\mathrm{Gr/SiO2}}$ is calculated as 3.2%. I is the laser intensity of 0.015 mW · μm^{-2}. The thermal conductance of SiO$_2$/Si interface is 4.2 × 10^7 W · m^{-2} · K^{-1} according to the literature [44]. The temperature of the surrounding boundary is set as ambient temperature. The temperature of the silicon top surface is set as the measured value of 305.2 ± 1.1 K.

In the simulation, the thermal conductance of Gr/SiO$_2$ interface is varied to best fit the measured temperature rise of graphene within the heated region. When the simulated average temperature rise of graphene approximates to $\Delta T_{\mathrm{Gr}} = 61.4 \pm 3.2$ K as shown in figure 5(b), the thermal conductance of Gr/SiO$_2$ interface of $7.7^{+0.7}_{-0.6} \times 10^3$ W · m^{-2} · K^{-1} is determined. The measured $G_{\mathrm{Gr/SiO2}}$ agrees with the reported value for the unconstrained graphene interface [35], which is far smaller than the sandwiched graphene interface [44].

3.3. Thermal conductance of Gr/Au interface

The FE simulation model of Gr/Au/Cr/SiO$_2$/Si is shown in figure 6(a). The model and simulation process are similar to that of Gr/SiO$_2$/Si case. A uniform heat source $\dot{q}_{\mathrm{Gr/Au}}$ is applied to graphene within the heated region expressed by $\dot{q}_{\mathrm{Gr/Au}} = \alpha_{\mathrm{Gr/Au}} I / t_{\mathrm{Gr}}$, where $\alpha_{\mathrm{Gr/Au}}$ is the absorptance of graphene on Au. The reflectance of gold is 0.7 [45] at the incident wavelength, and $\alpha_{\mathrm{Gr/Au}}$ is then calculated as 3.9%. I is 0.015 mW · μm^{-2}. The volumetric heat source applied to the Au has the expression of $\dot{q}_{\mathrm{Au}} = \alpha_{\mathrm{Au}}(1 - \alpha_{\mathrm{Gr/Au}}) I / t_{\mathrm{Au}}$, where α_{Au} is the absorptance of gold (0.3 [45]), t_{Au} is the thickness of Au (200 nm). The Au layer and Cr layer are prepared using sputter coating method, and the layers are assumed to well contact with the layer below themselves, so the thermal conductance of all the interfaces in Au/Cr/SiO$_2$/Si is defined to be 5.0 × 10^7 W · m^{-2} · K^{-1} [46]. The temperature of the silicon substrate's bottom surface is set to be the same as the surrounding boundary at 300 K.

When the simulated average temperature rise of graphene within the heated region approximates to the measured one ($\Delta T_{Gr} = 34.1 \pm 3.6$ K) as shown in figure 6(b), the thermal conductance of Gr/Au interface is $(1.7 \pm 0.2) \times 10^4$ W $\cdot$ m^{-2} $\cdot$ K^{-1}. Since the input temperature of silicon bottom surface in the simulation model is 300 K, which may be underestimated with respect to the actual case. The extracted value of $G_{Gr/Au}$ from simulation could be assumed as the lower limit. The order of magnitude of $G_{Gr/Au}$ approximates to $G_{Gr/SiO2}$ because of the same unconstrained state of graphene on the substrates.

3.4. Physical interpretation of differences between $G_{Gr/SiO2}$ and $G_{Gr/Au}$

In our experiment, the measured graphene samples are from the same batch, and supported on the substrates unconstrained. The experimental setup, the wavelength of the Raman excitation laser, and the power are all kept the same. Furthermore, the focal spot size ($\sim$50 μm) of the laser is large enough, and the measured results could well represent the average temperature rise in the irradiated area on the graphene. Thus, the measured $G_{Gr/SiO2}$ and $G_{Gr/Au}$ are comparable. They differ by up to one order of magnitude which originates in the same main thermal transport mechanism based on the transmission of acoustic phonons [7, 47] across the interface of the graphene with both metal and nonmetal.

However, $G_{Gr/Au}$ is a little larger than $G_{Gr/SiO2}$ with the consideration of the measurement uncertainty. It indicates more than one thermal transport mechanism occur in Gr/Au interface. Apparently, Au substrate is more thermally conductive compared with SiO$_2$ substrate. But, the measured $G_{Gr/Au}$ is just higher than twice of $G_{Gr/SiO2}$, largely different from the differences in thermal conductivity between Au and SiO$_2$. Therefore, the underlying mechanisms need to be explored. When the temperature of the substrate is higher than its Debye temperature, the inelastic scattering of phonons at the interface will increase and benefit the interfacial heat transfer [48, 49]. The Debye temperature of Au is 165 K, far lower than the room temperature and that of SiO$_2$ (550 K) [50] and graphene (2300 K [51]). The probability of multi-phonons inelastic scattering of Gr/Au interface is larger which contributes to the interfacial thermal transport. Besides, electrons are also involved in the heat conduction across Gr/Au interface which has been experimentally and theoretically studied by Zhang *et al* [52]. They found that the thermal conductance of Au/Gr/Au interface was decreased by 50% when the encased graphene was hydrogenated which was attributed to that the hydrogenation changed the electron band and resulted in closing the channel to interact with the free electrons in Au. Thus, with the contribution from electron scatterings and multi-phonons inelastic scatterings at the interface, the heat transfer across Gr/Au may be more efficient with respect to Gr/SiO$_2$ interface.

In addition, Raman spectra in figure 2 show that G band and 2D band of graphene on Au exhibits a redshift of 3 cm^{-1} and 8 cm^{-1}, respectively, with respect to the graphene on SiO$_2$. This is due to the charge transfer between graphene and Au [53], and the interaction between graphene and Au is different from that between graphene and SiO$_2$. The interfacial thermal conductance is found related to the adhesion force, mainly denoting the Van der Waals force, between graphene and the substrate. The increase in interfacial state force could decrease the distance between molecules and improve the interfacial thermal conductance [54], substantiated by the experimental observation of the interface between silicon nanotip and taC surface [55]. It has been measured recently that the adhesion energy of Gr/Au interface is 7687.10 mJ $\cdot$ m^{-2}, and is larger than that of Gr/SiO$_2$ (567.14 mJ $\cdot$ m^{-2}) [56–64]. A probably thinner spacing distance between graphene and Au than that between graphene and SiO$_2$ facilitates the heat transfer across the unconstrained graphene/metal interface and thus enhances $G_{Gr/Au}$. Interfacial heat transfer of graphene is also concerned with the material category of substrate beside the interfacial phonons transport.

4. Conclusion

The thermal conductance of the unconstrained graphene on SiO$_2$ and on Au is studied under the same experimental condition by using the steady-state Raman optothermal method. The thermal conductance is measured to be $7.7^{+0.7}_{-0.6} \times 10^3$ W $\cdot$ m^{-2} $\cdot$ K^{-1} for the unconstrained Gr/SiO$_2$ interface, and to be $1.7^{+0.2}_{-0.2} \times 10^4$ W $\cdot$ m^{-2} $\cdot$ K^{-1} for the unconstrained Gr/Au interface. As phonons are the main heat carriers for these two interfaces, the measured values are in the same order of magnitude. However, $G_{Gr/Au}$ is a little larger than $G_{Gr/SiO2}$. With the increased probability of multi-phonons inelastic scatterings due to the lower Debye temperature of Au than the ambient temperature and the additional contribution from electron scatterings, the interfacial heat transfer of Gr/Au is enhanced. Another reason is that the adhesion energy of Gr/Au interface is larger than that of Gr/SiO$_2$ interface, resulting in thinner spacing between graphene and Au and a higher thermal conductance of Gr/Au interface. Interfacial heat transfer of graphene is proved to be related to the substrate's material category, providing a foundation for understanding the interfacial heat transfer mechanism of two-dimensional atomic crystal material. The results also help for optimizing interfacial heat transfer by the

selection of substrate material category which benefits for the application of graphene into thermal management of electronic devices.

Acknowledgments

Conflicts of interest

There are no conflicts of interest to declare.

ORCID iDs

Yanan Yue ● https://orcid.org/0000-0002-3489-3949

References

[1] Balandin A A 2011 Thermal properties of graphene and nanostructured carbon materials *Nat. Mater.* **10** 569–81
[2] Yu W, Liu C, Qiu L, Zhang P, Ma W, Yue Y, Xie H and Larkin L S 2018 Advanced thermal interface materials for thermal management *Eng. Sci.* **2** 95
[3] Baringhaus J *et al* 2014 Exceptional ballistic transport in epitaxial graphene nanoribbons *Nature* **506** 349
[4] Chen J-H, Jang C, Xiao S, Ishigami M and Fuhrer M S 2008 Intrinsic and extrinsic performance limits of graphene devices on SiO_2 *Nat. Nanotechnol.* **3** 206
[5] Seol J H *et al* 2010 Two-dimensional phonon transport in supported graphene *Science* **328** 213
[6] Wang Y Y, Ni Z H, Yu T, Shen Z X, Wang H M, Wu Y H, Chen W and Shen Wee A T 2008 Raman studies of monolayer graphene: the substrate effect *J. Phys. Chem. C* **112** 10637–40
[7] Correa G C, Foss C J and Aksamija Z 2017 Interface thermal conductance of van der Waals monolayers on amorphous substrates *Nanotechnology* **28** 135402
[8] Song H, Liu J, Liu B, Wu J, Cheng H-M and Kang F 2018 Two-dimensional materials for thermal management applications *Joule* **2** 442
[9] Li M, Zhang J, Hu X and Yue Y 2015 Thermal transport across graphene/SiC interface: effects of atomic bond and crystallinity of substrate *Appl. Phys. A: Mater. Sci. Process.* **119** 415–24
[10] Jiang T, Zhang X, Vishwanath S, Mu X, Kanzyuba V, Sokolov D A, Ptasinska S, Go D B, Xing H G and Luo T 2016 Covalent bonding modulated graphene-metal interfacial thermal transport *Nanoscale* **8** 10993–1001
[11] Kim J Y, Lee J-H and Grossman J C 2012 Thermal transport in functionalized graphene *ACS Nano* **6** 9050–7
[12] Koh Y K, Lyons A S, Bae M-H, Huang B, Dorgan V E, Cahill D G and Pop E 2016 Role of remote interfacial phonon (RIP) scattering in heat transport across graphene/SiO_2 interfaces *Nano Lett.* **16** 6014–20
[13] Balandin A A, Ghosh S, Bao W, Calizo I, Teweldebrhan D, Miao F and Lau C N 2008 Superior thermal conductivity of single-layer graphene *Nano Lett.* **8** 902
[14] Li Q Y, Xia K, Zhang J, Zhang Y, Li Q, Takahashi K and Zhang X 2017 Measurement of specific heat and thermal conductivity of supported and suspended graphene by a comprehensive Raman optothermal method *Nanoscale* **9** 10784
[15] Wang H, Kurata K, Fukunaga T, Ago H, Takamatsu H, Zhang X, Ikuta T, Takahashi K, Nishiyama T and Takata Y 2016 Simultaneous measurement of electrical and thermal conductivities of suspended monolayer graphene *J. Appl. Phys.* **119** 244306
[16] Liu J-H, Xie H-H, Hu Y-D, Zhang X and Zhang Y-Y 2017 Thermal transport in suspended SWCNTs at high heat fluxes *Int. J. Heat Mass Transfer* **108** 572–6
[17] Liu J, Li T, Hu Y and Zhang X 2017 Benchmark study of the length dependent thermal conductivity of individual suspended, pristine SWCNTs *Nanoscale* **9** 1496–501
[18] Li Q-Y, Katakami K, Ikuta T, Kohno M, Zhang X and Takahashi K 2019 Measurement of thermal contact resistance between individual carbon fibers using a laser-flash Raman mapping method *Carbon* **141** 92–8
[19] Wang R, Wang T, Zobeiri H, Yuan P, Deng C, Yue Y, Xu S and Wang X 2018 Measurement of thermal conductivity of suspended MoS2 and MoSe2 by nanosecond ET-Raman free of temperature calibration and laser absorption evaluation *Nanoscale* **10** 23087
[20] Zobeiri H, Wang R, Zhang Q, Zhu G and Wang X 2019 Hot carrier transfer and phonon transport in suspended nm WS2 films *Acta Mater.* **175** 222–37
[21] Li Q-Y, Takahashi K and Zhang X 2019 Frequency-domain Raman method to measure thermal diffusivity of one-dimensional microfibers and nanowires *Int. J. Heat Mass Transfer* **134** 539–46
[22] Li Q-Y, Ma W-G and Zhang X 2016 Laser flash Raman spectroscopy method for characterizing thermal diffusivity of supported 2D nanomaterials *Int. J. Heat Mass Transfer* **95** 956–63
[23] Zobeiri H, Wang R, Wang T, Lin H, Deng C and Wang X 2019 Frequency-domain energy transport state-resolved Raman for measuring the thermal conductivity of suspended nm-thick MoSe2 *Int. J. Heat Mass Transfer* **133** 1074–85
[24] Xu S, Wang T, Hurley D, Yue Y and Wang X 2015 Development of time-domain differential Raman for transient thermal probing of materials *Opt. Express* **23** 10040–56
[25] Yue Y N, Zhang J C and Wang X W 2011 Micro/nanoscale spatial resolution temperature probing for the interfacial thermal characterization of epitaxial graphene on 4H-SiC *Small* **7** 3324
[26] Li C Z, Xu S, Yue Y N, Yang B and Wang X W 2016 Thermal characterization of carbon nanotube fiber by time-domain differential Raman *Carbon* **103** 101–8
[27] Sullivan S, Vallabhaneni A, Kholmanov I, Ruan X, Murthy J and Shi L 2017 Optical generation and detection of local nonequilibrium phonons in suspended graphene *Nano Lett.* **17** 2049–56

[28] Vallabhaneni A K, Singh D, Bao H, Murthy J and Ruan X 2016 Reliability of Raman measurements of thermal conductivity of single-layer graphene due to selective electron-phonon coupling: a first-principles study *Phys. Rev. B* **93** 125432

[29] An M, Song Q, Yu X, Meng H, Ma D, Li R, Jin Z, Huang B and Yang N 2017 Generalized two-temperature model for coupled phonons in nanosized graphene *Nano Lett.* **17** 5805–10

[30] Guermoune A, Chari T, Popescu F, Sabri S S, Guillemette J, Skulason H S, Szkopek T and Siaj M 2011 Chemical vapor deposition synthesis of graphene on copper with methanol, ethanol, and propanol precursors *Carbon* **49** 4204–10

[31] Kim K-S, Lee H-J, Lee C, Lee S-K, Jang H, Ahn J-H, Kim J-H and Lee H-J 2011 Chemical vapor deposition-grown graphene: the thinnest solid lubricant *ACS Nano* **5** 5107–14

[32] Ferrari A C *et al* 2006 Raman spectrum of graphene and graphene layers *Phys. Rev. Lett.* **97** 187401

[33] Telg H, Duque J G, Staiger M, Tu X, Hennrich F, Kappes M M, Zheng M, Maultzsch J, Thomsen C and Doorn S K 2012 Chiral index dependence of the G + and G– Raman modes in semiconducting carbon nanotubes *ACS Nano* **6** 904–11

[34] Graf D, Molitor F, Ensslin K, Stampfer C, Jungen A, Hierold C and Wirtz L 2007 Spatially resolved Raman spectroscopy of single- and few-layer graphene *Nano Lett.* **7** 238–42

[35] Tang X, Xu S, Zhang J and Wang X 2014 Five orders of magnitude reduction in energy coupling across corrugated graphene/substrate interfaces *ACS Appl. Mater. Interfaces* **6** 2809

[36] Xu C Y, Zhang P X and Yan L 2001 Blue shift of Raman peak from coated TiO2 nanoparticles *J. Raman Spectrosc.* **32** 862–5

[37] Menéndez J and Cardona M 1984 Temperature dependence of the first-order Raman scattering by phonons in Si, Ge, and α-Sn: anharmonic effects *Phys. Rev. B* **29** 2051–9

[38] Cai W, Moore A L, Zhu Y, Li X, Chen S, Shi L and Ruoff R S 2010 Thermal transport in suspended and supported monolayer graphene grown by chemical vapor deposition *Nano Lett.* **10** 1645–51

[39] Bolotin K I, Sikes K J, Jiang Z, Klima M, Fudenberg G, Hone J, Kim P and Stormer H L 2008 Ultrahigh electron mobility in suspended graphene *Solid State Commun.* **146** 351–5

[40] Suk J W, Kirk K, Hao Y, Hall N A and Ruoff R S 2012 Thermoacoustic sound generation from monolayer graphene for transparent and flexible sound sources *Adv. Mater.* **24** 6342–7

[41] Zhao W Q, Chen W, Yue Y N and Wu S J 2017 In-situ two-step Raman thermometry for thermal characterization of monolayer graphene interface material *Appl. Therm. Eng.* **113** 481

[42] Chien H-C, Yao D-J, Huang M-J and Chang T-Y 2008 Thermal conductivity measurement and interface thermal resistance estimation using SiO2 thin film *Rev. Sci. Instrum.* **79** 054902

[43] Nair R R, Blake P, Grigorenko A N, Novoselov K S, Booth T J, Stauber T, Peres N M R and Geim A K 2008 Fine structure constant defines visual transparency of graphene *Science* **320** 1308

[44] Yang J, Ziade E, Maragliano C, Crowder R, Wang X, Stefancich M, Chiesa M, Swan A K and Schmidt A J 2014 Thermal conductance imaging of graphene contacts *J. Appl. Phys.* **116** 023515

[45] Montecchi M and Masetti E 1991 Measurement of vibrational deexcitation efficiencies of gold, chromium, zinc selenide, and amorphous carbon thin films *Phys. Rev. B* **44** 11649–54

[46] Cahill D G, Bullen A and Seung-Min L 2000 Interface thermal conductance and the thermal conductivity of multilayer thin films *High Tem. - High Pressures* **32** 135–42

[47] Mao R, Kong B D, Gong C, Xu S, Jayasekera T, Cho K and Kim K W 2013 First-principles calculation of thermal transport in metal/graphene systems *Phys. Rev. B* **87** 165410

[48] Hopkins P E and Norris P M 2009 Relative contributions of inelastic and elastic diffuse phonon scattering to thermal boundary conductance across solid interfaces *J. Heat Transfer* **131** 022402

[49] Zhang C W, Bi K D, Wang J L, Ni Z H and Chen Y F 2012 Measurement of thermal boundary conductance between metal and dielectric materials using femtosecond laser transient thermoreflectance technique *Sci China Tech. Sci.* **42** 597–602

[50] Lyeo H-K and Cahill D G 2006 Thermal conductance of interfaces between highly dissimilar materials *Phys. Rev. B* **73** 144301

[51] Tewary V K and Yang B 2009 Singular behavior of the Debye-Waller factor of graphene *Phys. Rev. B* **79** 125416

[52] Zhang C *et al* 2017 Electron contributions to the heat conduction across Au/graphene/Au interfaces *Carbon* **115** 665–71

[53] Sutrová V, Šloufová I, Melníková Z, Kalbáč M, Pavlova E and Vlčková B 2017 Effect of ethanethiolate spacer on morphology and optical responses of Ag nanoparticle array–single layer graphene hybrid systems *Langmuir* **33** 14414–24

[54] Prasher R 2018 Acoustic mismatch model for thermal contact conductance of van der Waals contacts under static force *Nanoscale and Microscale Thermophys. Eng.* **22** 1

[55] Gotsmann B and Lantz M A 2012 Quantized thermal transport across contacts of rough surfaces *Nat. Mater.* **12** 59

[56] Torres J, Zhu Y, Liu P, Lim S C and Yun M 2018 Adhesion energies of 2D graphene and MoS2 to silicon and metal substrates *Phys. Status Solidi a* **215** 1700512

[57] Paek E and Hwang G S 2013 A computational analysis of graphene adhesion on amorphous silica *J. Appl. Phys.* **113** 164901

[58] Fan X F, Zheng W T, Chihaia V, Shen Z X and Kuo J-L 2012 Interaction between graphene and the surface of SiO2 *J. Phys. Condens. Matter* **24** 305004

[59] Wei G, Penghao X, Graeme H, Kenneth M L and Rui H 2014 Interfacial adhesion between graphene and silicon dioxide by density functional theory with van der Waals corrections *J. Phys. D: Appl. Phys.* **47** 255301

[60] Zong Z, Chen C-L, Dokmeci M R and Wan K-T 2010 Direct measurement of graphene adhesion on silicon surface by intercalation of nanoparticles *J. Appl. Phys.* **107** 026104

[61] Boddeti N G, Koenig S P, Long R, Xiao J, Bunch J S and Dunn M L 2013 Mechanics of adhered, pressurized graphene blisters *J. Appl. Mech.* **80** 040909

[62] Na S R, Suk J W, Ruoff R S, Huang R and Liechti K M 2014 Ultra long-range interactions between large area graphene and silicon *ACS Nano* **8** 11234–42

[63] Jiang T and Zhu Y 2015 Measuring graphene adhesion using atomic force microscopy with a microsphere tip *Nanoscale* **7** 10760–6

[64] Das S, Lahiri D, Lee D-Y, Agarwal A and Choi W 2013 Measurements of the adhesion energy of graphene to metallic substrates *Carbon* **59** 121–9